This document is a preprint of: T. Pham, R. Bomfin, A. Nimr et al., "Joint Communications and Sensing Experiments Using mmWave Platforms," in Proceedings of 2021 IEEE 22nd International Workshop on Signal Processing Advances in Wireless Communications (SPAWC 2021), Lucca, Italy, (pp. 501-505), Sep 2021. DOI:10.1109/SPAWC51858.2021.9593174

Joint Communications and Sensing Experiments Using mmWave Platforms

Thuy M. Pham*, Roberto Bomfin†, Ahmad Nimr†, Andre N. Barreto*, Padmanava Sen*, Gerhard Fettweis*†
*Barkhausen Institut, Dresden, Germany
{minhthuy.pham, andre.nollbarreto, padmanava.sen, gerhard.fettweis}@barkhauseninstitut.org
†Technische Universität Dresden, Germany
{roberto.bomfin, ahmad.nimr, gerhard.fettweis}@tu-dresden.de

***Abstract*—Joint communications and radar sensing (JC&S) is expected to be one of the key features in next-generation wireless communication systems, and one of the main enablers for this is the availability of very wide bands in the millimeter-wave (mmWave) frequencies. Most of the literature has investigated different aspects of JC&S by means of theoretical or simulation studies. However, before this concept is fully understood and applied in practice, prototyping and large-scale experiments are needed. In this paper, we present two mmWave demonstration testbeds and discuss the measurement results for JC&S.**

***Index Terms*—communications, sensing, JC&S, mmWave, testbeds.**

I. Introduction

Joint communications and sensing systems (JC&S) have attracted a lot of attention in recent years [1]–[6]. Such systems are expected to mitigate the spectrum scarcity problem and to enable usage of the radio resources as well as the hardware more efficiently. However, the different specifications of communications and radar systems also pose challenges to this joint design.

Most of the research in this field has concentrated either on the design of waveforms or on investigating different signal processing techniques [1], [3]–[6]. However, the prototyping of JC&S systems, especially at mmWave frequency bands, is still very limited in the literature [7], [8].

In this paper we describe experimental platforms that were deployed in our premises to test and validate JC&S concepts. We used two different setups: a beamforming setup at 26 GHz and a 71–76 GHz E-band setup, both using frequency-modulated continuous wave (FMCW), or chirps, as waveforms, as they offer good radar detection properties and efficient hardware implementation, and are, for these reasons, commonly employed in existing radar systems. Chirps can also be employed for communications [9], and both setups are also capable of characterizing communication links [10], [11].

The beamforming setup is used in one of the 5G mmWave bands for demonstrating angle detection based on beam steering. Section II-A presents a theoretical overview of beamforming for mmWave radar, and a hardware setup for beamforming studies at 26 GHz is described in Section III-A. The related angle detection results are discussed in Section IV-A.

The E-band setup demonstrates GHz-bandwidth radar detection and communication using modulated chirps. In Section II-B a chirp-based waveform for JC&S is discussed. Section III-B describes the 71–76 GHz setup, and the radar detection results are presented in IV-B.

II. Overview

A. Radar with mmWave and beamforming

Consider a uniform linear array (ULA) of antennas with N_{T} elements spaced by Δ, such that the array steering vector is $\boldsymbol{a}(\theta) \in \mathbb{C}^{N_{\mathrm{T}}\times 1}$, $[\boldsymbol{a}(\theta)]_{(n_{\mathrm{t}})} = e^{-j2\pi n_{\mathrm{t}}\frac{\Delta}{\lambda}\sin(\theta)}$, for $n_{\mathrm{t}} = 0, 1, \cdots, N_{\mathrm{T}}–1$. In analog and hybrid beamforming, an orthogonal codebook $\boldsymbol{W} \in \mathbb{C}^{N_{\mathrm{T}}\times N_{\mathrm{T}}}$ can be designed [12] to provide spatial resources for serving the data communications of multiple users. The radiation pattern of the i-th beam is $A(\theta, i) = \boldsymbol{a}^T(\theta)\boldsymbol{w}_i$, where $\boldsymbol{w}_i \in \mathbb{C}^{N_{\mathrm{T}}\times 1}$ is the i-th beam. We employ a low-complexity analog codebook design, in which a Butler-matrix phase-shift network connects N_{T} signals ports to the antenna array using delay lines forming fast Fourier transform (FFT) butterfly graph. Therefore, $[\boldsymbol{w}_i]_{(n_{\mathrm{t}})} = e^{j2\pi n_{\mathrm{t}}\frac{i-0.5-N_{\mathrm{T}}/2}{N_{\mathrm{T}}}}$, $i = 1 \cdots N_{\mathrm{T}}$.

The beams can be shared for simultaneous communications and radar in different directions [13]. Moreover, the radar function can be integrated with the beam search to construct a radio map that can be used to reduce the beam training overhead [14]. We consider a mono-static radar system, where the transmit (Tx) and receive (Rx) front-ends are collocated and tuned to the same beam. The area is scanned by transmitting a probing signal, whose baseband representation is denoted as $x(t)$. For a given beam, the baseband received signal, after propagation through P paths, is given by

$$y_i(t) = \sum_{p=1}^{P} \underbrace{\rho_p e^{\phi_p} \boldsymbol{w}_i^H \boldsymbol{a}(\theta_p)\boldsymbol{a}^T(\theta_p)\boldsymbol{w}_i}_{h_{i,p}} x(t-\tau_p) + z_i(t) + v_i(t), \tag{1}$$

where ρ_p is a gain that depends on the antenna gains, on the transmit power, on the p-th reflector geometry and on the distance d_p between the reflector and the transmitter. Moreover, θ_p denotes the angle, and $\tau_p = 2\frac{d_p}{c}$ is the delay. $v_i(t)$ denotes the additive noise, and $z_i(t)$ the self-interference, arising from a leakage of the transmit signal. The overall complex gain for path p is denoted as $h_{i,p}$. The angular resolution depends on the beam width, which is influenced by the number of antennas and their patterns. In general, increasing the number of antennas in the ULA increases the

This document is a preprint of: T. Pham, R. Bomfin, A. Nimr et al., "Joint Communications and Sensing Experiments Using mmWave Platforms," in Proceedings of 2021 IEEE 22nd International Workshop on Signal Processing Advances in Wireless Communications (SPAWC 2021), Lucca, Italy, (pp. 501-505), Sep 2021. DOI:10.1109/SPAWC51858.2021.9593174

angular resolution. The range estimation resolution depends on the signal bandwidth, i.e., $\Delta d_p = \frac{c}{2B}$. For instance, 150 MHz are needed to achieve a resolution of 1 m. Therefore, a narrowband signal can be first used to scan for targets in the space. Once targets are detected in a certain beam, the beam switches to wideband fine resolution mode. The self-interference can be expressed as $z_i(t) = h_{i,0}x(t)$, where $h_{i,0}$ is an attenuation factor. Thus, the discrete signal can be expressed as

$$y_i[n] = \sum_{l=0}^{L-1} h[l]x[n-l] + v_i[n], \tag{2}$$

where $h[l]$ is the discrete channel corresponding to

$$h[l] = \sum_{p=0}^{P} h_{i,p}\beta\left(\frac{l}{F_s} - \tau_p\right). \tag{3}$$

Here, $\beta(\tau)$ is the impulse response of the baseband transmission low-pass (LP) filter , and F_s is the sampling frequency.

In this paper, we focus on detecting the targets with narrowband signals, such that there is only one significant channel tap, i.e. $y_i[n] = hx[n] + v_i[n]$.

B. Waveforms for JC&S

Here we present the waveform that is used in the mmWave setup. A joint design of communications and radar system allows a more efficient use of spectrum and hardware resources. However, different requirements between radar and communications systems make the design of a single waveform for both applications quite challenging. In fact, the majority of existing approaches exploit modifications of either communications or radar waveforms for the co-design [1], [5], [8], [15], [16]. Others investigate the possibilities to design the waveform flexibly without relying on traditional communications or radar waveforms [2], [7].

A widely used communications-based method is to utilize orthogonal frequency-division multiplexing (OFDM) signalling for radar [1], [15]. However, the performance is slightly degraded with this approach in comparison with dedicated radar waveforms [4], [17]. For instance, the authors in [17] have shown that OFDM-based radar is more susceptible to interference compared with FMCW, which is traditionally used for radar system, especially automotive applications. When compared with FMCW, OFDM also requires a more complex transceiver for several reasons: i) it has a higher peak-to-average power ratio (PAPR); ii) because of the required digital processing, a higher sampling rate at the analog-to-digital converter (ADC) is required; and iii) it requires a better rejection of the self-interference, demanding a full-duplex transceiver. Moreover, the communications systems aim at maximizing information-theoretic capacity, thus employing techniques enhancing the capacity of the communications systems, such as beamforming, which was explained in Section II-A. This may, on the one hand, make target detection harder in case of radar systems, but, on the other hand, allow for a better spatial resolution.

Another common alternative is to embed communications signals into traditional radar waveforms [5], [8]. In general, this method cannot support high-data-rate transmission without several major modifications. For instance, the authors in [5], [8] have employed the chirp sequence as a carrier and modulated the communications symbols by frequency shift keying (FSK). However, this approach comes at a cost of a lower spectral efficiency. This problem can be solved efficiently by higher modulation orders and/or by overlapping several chirps to increase the spectral efficiency while preserving the good properties of chirps for sensing. In fact, a study in [9] shows that we can transmit at the Nyquist signalling rate or higher for chirp-based communications using proper equalization methods.

An emerging approach that can trade off the requirements of both communications and radar without being constrained to the existing systems is to design JC&S systems at mmWave frequency. The fact that this frequency band provides not only larger bandwidth but also finer resolution, thus has great potential for both high-data-rate communications and high-accuracy sensing. In fact, the demonstration or deployment of this approach is still limited partially due to cost and hardware capability [6], [7], [18], [19]. In this regard, our research helps to demonstrate the concept and contribute to the understanding of the performance of the mmWave JC&S in practice.

In our mmWave JC&S testbed we follow the approach of modulating chirps for communications, with a series of unmodulated non-overlapping chirps transmitted in the beginning of the frame [20]. More specifically, we consider binary phase shift keying (BPSK) modulation for the communications and the modulated signal is defined as $u(t) = \xi s(t)$ where $\xi = \pm 1$ and $s(t) = \sqrt{\frac{E_b}{\tau_d}}e^{j\pi\mu t^2}, \quad |t| \leq \frac{\tau_d}{2}$ is a complex baseband chirp signal; E_b and μ are the symbol energy and the chirp slope, respectively; B is the bandwidth and τ_d is the chirp duration. As a result, we can express the joint radar and communications signal as follows

$$w(t) = \underbrace{\sum_{m=0}^{(\iota-1)} s(t - m\tau_d)}_{\text{Radar}} + \underbrace{\sum_{k=0}^{(\kappa-1)} u(t - \iota\tau_d - k\tau_d)}_{\text{Communications}}, \tag{4}$$

where the first summation and the second one are for the radar and communications, respectively. The former is then used both for channel estimation in the communications link and for radar detection. At the receiver, we may express the filter output as

$$y[n[= w[n] \circledast h[n], \tag{5}$$

where the impulse response $h[n]$ represents channel and receive filter. Note that we present only the performance of radar detection of two testbeds in this paper due to space limitation.

III. Demonstration Platforms

A. 26 GHz mmWave

1) Hardware Setup: We use a similar setup as in [21], which employs the beamforming Butler matrix developed in

This document is a preprint of: T. Pham, R. Bomfin, A. Nimr et al., "Joint Communications and Sensing Experiments Using mmWave Platforms," in Proceedings of 2021 IEEE 22nd International Workshop on Signal Processing Advances in Wireless Communications (SPAWC 2021), Lucca, Italy, (pp. 501-505), Sep 2021. DOI:10.1109/SPAWC51858.2021.9593174

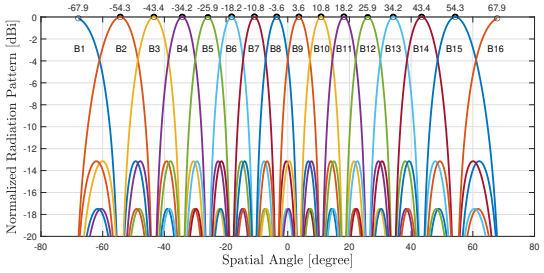

Fig. 1. Beams radiation patterns.

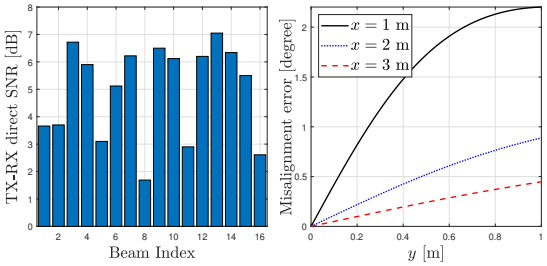

Fig. 2. Measured SNR of direct link and misalignment error corresponding to the locations of Tx: $(0,\ 0,\ 0.85)$ and Rx :$(-0.08,\ 0,\ 0.35)$.

[10]. This matrix consists of $N_{\mathrm{t}} = 16$ signal ports connected to a ULA of $N_{\mathrm{T}} = 16$ quasi-yagi antenna elements with half-wavelength spacing. A fixed beam is associated with each signal port, enabling a simplified beam switching. The radiation pattern of individual beams is shown in Fig. 1. However, that system has been tested for communications only, and, in this paper, we evaluate the sensing function as a preliminary step before elaborating further JC&S approaches. As sketched in Fig. 3, the system consists of the baseband unit, which is a mixture of FPGA and PC responsible for the digital signal processing. The intermediate frequency (IF) signal is processed with the radio frequency (RF) frontend of *Ettus* USRP X310 software defined radio (SDR) platform, which provides digital interface to the baseband unit, and coaxial cable interface to the mmWave front-end. The Tx mmWave front-end converts the IF signal centered at $f_{\mathrm{IF}} = 2.4$ GHz to the carrier frequency of the Butler matrix $f_c = 26$ GHz. The up-converted signal is routed to the antenna elements after being amplified with a power amplifier (PA). The Rx fronted amplifies the signals received at each antenna by means of a low noise amplifier (LNA), the output signal of the Butler matrix is converted to the IF signal.

The Tx and Rx antennas are collocated and aligned along the z-axes with a spacing of 50 cm to reduce the cross talk, which is further reduced by shifting the Rx array along the x-axes by -8 cm at the expense of angular misalignment between transmitter (TX) and receiver (RX), since ideally both antennas should be at the same x-axes. In the right side of Fig. 2, we evaluate the misalignment error for a fixed target at located at (x, y) within the area in which the experiments are performed. The graph shows that the angular error is less than 2° in that area. With this setting, the signal-to-noise ratio (SNR) of the direct Tx-Rx link is less than 7 dB when there is no target.

2) Transmitted Signal and SNR Estimation: The sequence used in the 26 GHz system is similar to the one used in the channel sounding measurements of the Online Wireless Testbed [22] located at the TU Dresden. This signal consists of a sequence of down-chirps, up-chirps and zeros. The chirps are followed by a sequence of zeros that is used to estimate the noise level, and, consequently, the SNR can be measured. A very similar configuration of the channel sounding measurements of [22] is used. In particular, 5 sequences with 64 baseband samples of down and up-chirps are followed by

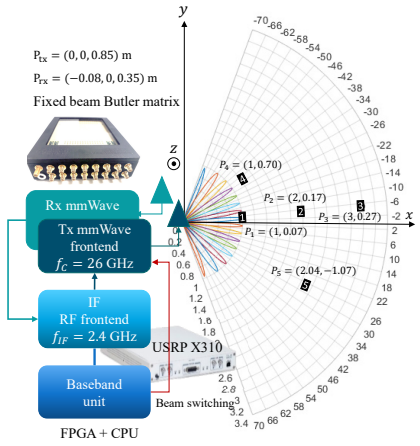

Fig. 3. 26 GHz mmWave setup for Radar function.

a sequence of 320 zeros samples. In this setup, one chirp sequence is generated based on the Zadoff-Chu sequence. The only modification from [22] is that here a cyclic prefix (CP) of 16 samples is introduced before the first down- and up-chirp sequences, respectively.

In summary, in the radar experiment of this paper, we employ the aforementioned chirp sequences and SNR estimation approach of [22] for each beam combination of the monostatic radar setup depicted in Fig. 3. In this way, the transmit signal is reflected with relatively high power when there is a target in a given angle, which can be detected by the SNR estimation.

B. 71-76 GHz E-band

In this subsection, we describe the hardware and software utilized for our proof-of-concept at E-band. More specifically, we use a NI mmWave system consisting of two PCI extensions for instrumentation (PXIs): one has a combined transmitter and a radar receiver, the other is a communications receiver. The transmitter and the receivers are connected to E-band mmWave heads (see Fig. 4). The code and the firmware are developed in Python and LabView, respectively.

The measurement setup is shown in Fig. 4. The setup consists of NI 3647 TX (71 to 76 GHz Up converter), NI 3657 RX (71 to 76 GHz Down converter), PXIe-3620 (8.5 to 13.5 GHz IQ modulator/demodulator), PXIe-3610 (baseband

This document is a preprint of: T. Pham, R. Bomfin, A. Nimr et al., "Joint Communications and Sensing Experiments Using mmWave Platforms," in Proceedings of 2021 IEEE 22nd International Workshop on Signal Processing Advances in Wireless Communications (SPAWC 2021), Lucca, Italy, (pp. 501-505), Sep 2021. DOI:10.1109/SPAWC51858.2021.9593174

generator), PXIe-3630 (baseband digitizer) and PXIe-7902 (FPGA processing unit). The system is integrated with NOFFZ application programming interface (API) and controlled by Python programs developed jointly by NOFFZ technologies and the Barkhausen Institut. The sampling rate supported by PXIe-3630 and PXIe-3610 is 3.072 GS/s and the maximum bandwidth supported meeting all specifications given in datasheet [11] is 2 GHz. The mmWave heads are connected to WR-12 pyramid horn antennas (SAR-1532-12-S2) from Eravant. The antennas with typical 15dBi gain have 3-dB beam bandwidths of 30° and 32° in E-plane and H-plane, respectively.

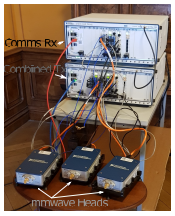

Fig. 4. Set up of mmWave transceiver system at 71-76 GHz

Fig. 5. Experimental scenario for E-band

IV. Measurement Results

A. Detection of target direction in 26 GHz

The goal of this experiment is to check the visibility and challenges of using the 26 GHz mmWave platform for radar detection. In this initial result, we focus on scanning to detect the existence of targets and measure the SNR corresponding to the reflected signal, as described in Subsection III-A, where a relatively small bandwidth of 10 MHz has been considered. The results are shown in Fig. 6, where 5 scans are performed. In each scan a target is placed in a different position, as illustrated in Fig. 3. In each scan, the SNR is measured for each beam. As it can be seen, when there is a target in the given beam direction, the SNR significantly increases. Although the SNR increases when the target is closer, it is difficult to accurately determine the distance with respect to the reference point, because the gain also depends on the alignment with the center of the beam and on the radar cross-section of the target. For instance, the measured SNR is 21.4 dB for the target placed at position P_1, which is distanced by 1 m from the radar unit, whereas at position P_2, with 2 m distance, the SNR drops by 3.7 dB in comparison to P_1. At P_3, distanced by 3 m, the SNR drops 7.3 dB in relation to P_1. As expected, the target at positions P_1, P_2 and P_3 produces a high SNR with beam 8, which has a small angle deviation from the center. Regarding points P_4 and P_5, the reflected signal returns with high SNR at beams number 4 and 12, respectively, which matches the position of the targets.

Another interesting outcome of this experiment is that the threshold for correct decision can be determined. As one can observe from Fig. 6, this threshold is approximately 9 dB such that the reflected signal has significantly more power than the self interference. That is, even where there is no target

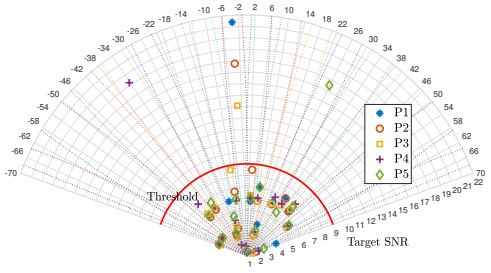

Fig. 6. SNR of scanned beams. A target is placed at a position P_x, and the SNRs measured by all beams are shown.

TABLE I
Experimental parameters

Parameters	Value
Chirp bandwidth	500 MHz
Chirp duration	$1\mu s$
Carrier frequency	73.5 GHz
Sampling frequency	1 GHz
Transmit gain	-20 to 25 dB
Attenuation	52.6 dB
Cable loss	3.87 dB
Receive gain	45 dB
No. of preambles	8
No. of communications chirps	50

at a particular direction, there is still a considerable amount of signal which excited the receive mmWave antenna. The high self-interference makes it harder to accurately detect targets at larger distances with narrow band probing signal.

In summary, these outcomes reveal that the 26 GHz mmWave radar is applicable to target detection in the angle domain. Nevertheless, this setup can be extended to estimate the distance of the target, by increasing the transmit bandwidth. In this case, a second tap of the discrete channel can be theoretically estimated, whose position is proportional to the target distance, while the first tap corresponds to the self-interference.

B. E-band object detection

In this subsection, we provide some results regarding the radar detection utilizing the platform at E-band. We use a number of chirps for radar and the rest are modulated for communications. For simplicity, we implemented BPSK-modulated chirps for communications and the cell-averaging constant false alarm rate (CA-CFAR) for radar. Note that the input of the detector is the output of the match filter and thus CA-CFAR is performed over the range. In the following, we show some initial results regarding radar detection at mmWave frequency. The experiments were carried out near the corner of the lab, which has less clutter. We placed a reflector around 1.5 m away from the transmitter (see Fig. 5). The number of reference cells and the guard cells for CA-CFAR detection were set at 10 and 2, respectively. The other parameters are detailed in Table I and the results are averaged over a large number of experiments i.e., 1000. An attenuator is placed between IF and RF stage in the transmitter chain and the cable loss incurred from that connection is taken into consideration and is given in Table I.

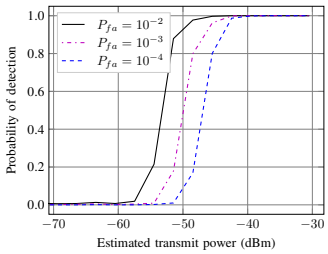

Fig. 7. Probability of detection with varying values of false alarm rate P_{fa}.

In Fig. 7, we study the performance of the radar detection using our aforementioned platform. Note that the probability of detection is given by

$$P_D = \frac{N_D}{N_T} \tag{6}$$

where N_D and N_T represent the number of detected objects and all the possible objects, respectively. As it can be seen in Fig. 7, all the curves change from undetected state to detected ones upon increasing the transmit power. Unsurprisingly, the detection curves, as expected, move to a higher-power regime when the false alarm rate decreases. As a result, our implementation shows consistent results with that of the literature [23], [24].

Taking advantage of our implementation, we aim at addressing the challenges of mmWave systems such as path loss, synchronization, channel estimation as well as other RF impairments in the future work.

V. Conclusion

In this paper, we have presented our proof-of-concept validation platforms for joint communications and sensing systems, especially at mmWave bands. Initial results have shown a good agreement with the existing literature. In fact, the platforms will assist us to investigate intensively the performance of the joint systems in practice. More importantly, we can utilize our implementations to study the effects of a real-life hardware and environment at mmWave frequencies, as well as to develop solutions to these challenges.

Acknowledgement

This research was financed by public funding of the state of Saxony, Germany. The authors would like to acknowledge the assistance of Paul Kühne and Maximilian Matthé in setting up the mmWave measurement system.

References

[1] S. H. Dokhanchi, M. R. B. Shankar, T. Stifter, and B. Ottersten, "OFDM-based automotive joint radar-communication system," in *Proc. IEEE RadarConf*, 2018.

[2] F. Liu, L. Zhou, C. Masouros, A. Li, W. Luo, and A. Petropulu, "Toward dual-functional radar-communication systems: Optimal waveform design," *IEEE Trans. Signal Process.*, vol. 66, no. 16, pp. 4264–4279, 2018.

[3] Y. Luo, J. A. Zhang, W. Ni, J. Pan, and X. Huang, "Constrained multibeam optimization for joint communication and radio sensing," in *Proc. IEEE GLOBECOM*, 2019.

[4] F. Liu, C. Masouros, A. Li, H. Sun, and L. Hanzo, "MU-MIMO communications with MIMO radar: From co-existence to joint transmission," *IEEE Trans. Wireless Commun.*, vol. 17, no. 4, pp. 2755–2770, 2018.

[5] S. Dwivedi, A. N. Barreto, P. Sen, and G. Fettweis, "Target detection in joint frequency modulated continuous wave FMCW radar-communication system," in *Proc. IEEE ISWCS*, 2019, pp. 277–282.

[6] K. V. Mishra, M. R. Bhavani Shankar, V. Koivunen, B. Ottersten, and S. A. Vorobyov, "Toward millimeter-wave joint radar communications: A signal processing perspective," *IEEE Signal Process. Mag.*, vol. 36, no. 5, pp. 100–114, 2019.

[7] P. Kumari, S. A. Vorobyov, and R. W. Heath, "Adaptive virtual waveform design for millimeter-wave joint communication–radar," *IEEE Trans. Signal Process.*, vol. 68, pp. 715–730, 2020.

[8] M. B. Alabd, L. G. de Oliveira, B. Nuss, W. Wiesbeck, and T. Zwick, "Time-frequency shift modulation for chirp sequence based radar communications," in *Proc. IEEE ICMIM*, 2020.

[9] T. M. Pham, A. N. Barreto, and G. P. Fettweis, "Efficient communications for overlapped chirp-based systems," *IEEE Wireless Commun. Lett.*, vol. 9, no. 12, pp. 2202–2206, 2020.

[10] X. Wang, M. Laabs, D. Plettermeier, K. Kosaka, and Y. Matsunaga, "MIMO antenna array system with integrated 16x16 Butler matrix and power amplifiers for 28ghz wireless communication," in *Proc. 12th German Microwave Conference (GeMiC)*, Mar. 2019, pp. 127–130.

[11] NI. [Online]. Available: http://www.ni.com/pdf/datasheet/us/71_76_GHz_Millimeter_Wave_Transceiver_System.pdf

[12] H.-L. Chiang, W. Rave, T. Kadur, and G. Fettweis, "A low-complexity beamforming method by orthogonal codebooks for millimeter wave links," in *Proc. IEEE ICASSP*, New Orleans, USA, May 2017.

[13] J. A. Zhang, X. Huang, Y. J. Guo, J. Yuan, and R. W. Heath, "Multibeam for joint communication and radar sensing using steerable analog antenna arrays," *IEEE Trans. Veh. Technol.*, vol. 68, no. 1, pp. 671–685, 2019.

[14] C. Jiao, Z. Zhang, C. Zhong, and Z. Feng, "An indoor mmwave joint radar and communication system with active channel perception," in *Proc. IEEE ICC*, 2018.

[15] J. R. Krier, M. C. Norko, J. T. Reed, R. J. Baxley, A. D. Lanterman, Xiaoli Ma, and J. R. Barry, "Performance bounds for an OFDM-based joint radar and communications system," in *Proc. IEEE MILCOM*, 2015, pp. 511–516.

[16] L. Gaudio, M. Kobayashi, G. Caire, and G. Colavolpe, "On the effectiveness of OTFS for joint radar parameter estimation and communication," *IEEE Trans. Wireless Commun.*, vol. 19, no. 9, pp. 5951–5965, 2020.

[17] G. K. Carvajal, M. F. Keskin, C. Aydogdu, O. Eriksson, H. Herbertsson, H. Hellsten, E. Nilsson, M. Rydström, K. Vänas, and H. Wymeersch, "Comparison of automotive FMCW and OFDM radar under interference," in *Proc. IEEE RadarConf*, 2020, pp. 1–6.

[18] R. M. Gutierrez, H. Yu, A. R. Chiriyath, G. Gubash, A. Herschfelt, and D. W. Bliss, "Joint sensing and communications multiple-access system design and experimental characterization," in *Proc. IEEE Aerospace Conference*, 2019, pp. 1–8.

[19] C. B. Barneto, S. D. Liyanaarachchi, M. Heino, T. Riihonen, and M. Valkama, "Full duplex radio/radar technology: The enabler for advanced joint communication and sensing," *IEEE Wireless Commun.*, vol. 28, no. 1, pp. 82–88, 2021.

[20] A. Barreto, T. Pham, S. George, P. Sen, and G. Fettweis, "Analysis of a chirp-based waveform for joint communications and radar sensing (JC&S) using non-linear components," in *Proc. IEEE EuCAP*, 2021.

[21] M. Danneberg, R. Bomfin, A. Nimr, Z. Li, and G. Fettweis, "USRP-based platform for 26/28 GHz mmwave experimentation," in *Proc. IEEE WCNCW*, Seoul, South Korea, Apr. 2020.

[22] M. Danneberg, R. Bomfin, S. Ehsanfar, A. Nimr, Z. Lin, M. Chafii, and G. Fettweis, "Online wireless lab testbed," in *Proc. IEEE WCNCW*, 2019.

[23] M. Richards, *Fundamentals Of Radar Signal Processing*. McGraw-Hill Education (India) Pvt Limited, 2005.

[24] R. Liu, D. Wang, P. Jia, and H. Sun, "An omnidirectional morphological method for aerial point target detection based on infrared dual-band model," *Remote Sensing*, vol. 10, no. 7, 2018.